Structural and Functional Insights into Depulfavirine as an HIV-1 RT Inhibitor

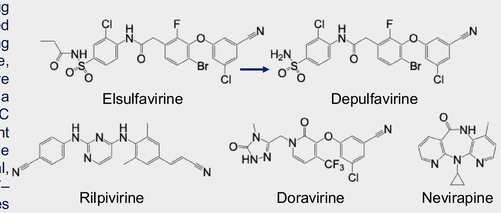
Alexa A. Snyder [1,2], Isabella L. Kaufman[1,2], Karen A. Kirby[1,2], Stefan G. Sarafianos[1,2]*

Background/Significance

Non-nucleoside reverse transcriptase inhibitors (NNRTIs) remain a key component of combination antiretroviral therapy (ART) for HIV-1 (1), yet drug resistance and the limited availability of long-acting options highlight the need for next-generation NNRTIs (2,3). As of 2024, ~40.8 million people are living with HIV-1 worldwide, and treatment-experienced individuals require durable, resistance-resilient therapies (4). Depulfavirine (VM1500A), the active metabolite of elsulfavirine (ESV), is a potent NNRTI being developed as a long-acting injectable; ESV is approved for oral use in Russia and EurAsEC countries (5,6). VM1500A retains activity against >90% of NNRTI-resistant isolates, including K103N and Y181C, with resistance requiring multiple mutations that often reduce viral fitness (7). We define the structural, biochemical, and virological basis of VM1500A activity through a 2.45 Å RT–VM1500A crystal structure, resistance profiling, and combination studies demonstrating additive to near-synergistic activity with clinically relevant antiretrovirals, including long-acting agents (8–10).

Why This Matters:

Depulfavirine combines strong resistance coverage, long-acting potential, and compatibility with existing combination regimens, supporting its development as a durable NNRTI for future HIV-1 treatment strategies.



Scheme 1. Chemical structures of NNRTIs. Elsulfavirine (ESV; prodrug of depulfavirine), depulfavirine (VM1500A), doravirine (DOR), rilpivirine (RPV), and nevirapine (NVP).

Methods

Structural Studies

- Recombinant HIV-1 reverse transcriptase (RT) was expressed and purified as previously described (11,12). RT–VM1500A complexes were crystallized, and the structure was solved at 2.45 Å resolution using X-ray diffraction data collected at APS beamline 22-ID-D, followed by molecular replacement and refinement with standard crystallographic software (13-17).

Biochemical Assays

- Polymerase inhibition was evaluated using purified wild-type and NNRTI-resistant HIV-1 RT variants in primer-extension assays to determine IC_{50} values for depulfavirine.

Virological and Combination Assays

- Antiviral activity, resistance profiling, and combination studies were performed using NL4-3Δenv VSV-G–pseudotyped virus in TZM-GFP cells. Combination activity with clinically relevant antiretrovirals was assessed using dose-matrix assays and analyzed with SynergyFinder Plus (18).

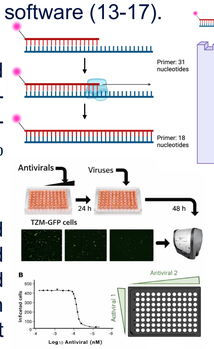


Figure 1. Primer extension assay to assess inhibition of HIV-1 reverse transcriptase activity. A 5'-Cy3–labeled DNA primer (18 nt) was annealed to a complementary DNA template to generate a primer–template substrate. Primer extension was initiated by incubation with wild-type or NNRTI-resistant HIV-1 reverse transcriptase in the presence of all four dNTPs and increasing concentrations of depulfavirine. Reaction products were resolved by denaturing polyacrylamide gel electrophoresis and visualized by fluorescence imaging. Fully extended products and unextended products were quantified to determine the extent of polymerase inhibition. Representative gel images illustrate dose-dependent inhibition of primer extension, which was used to calculate IC_{50} values for depulfavirine against wild-type and mutant RT variants.

Figure 2. Workflow for antiviral and combination assays in TZM-GFP cells.
(A) TZM-GFP cells were seeded in 96-well plates and pre-treated with antiviral compounds for 24 h prior to infection with NL4-3Δenv VSV-G–pseudotyped HIV-1. Cells were incubated for an additional 48 h, after which infection levels were quantified by automated fluorescence imaging of GFP-positive cells. Representative fluorescence images illustrate infection levels across drug concentrations.
(B) Antiviral activity and combination studies were performed using two-fold serial dilutions arranged in single-drug or dose-matrix formats. Infection levels were normalized to no-drug controls for synergy analysis.

Structural Insights Into Depulfavirine as an HIV-1 RT Inhibitor

2.4 Å Structure of WT HIV-1 in Complex with Depulfavirine

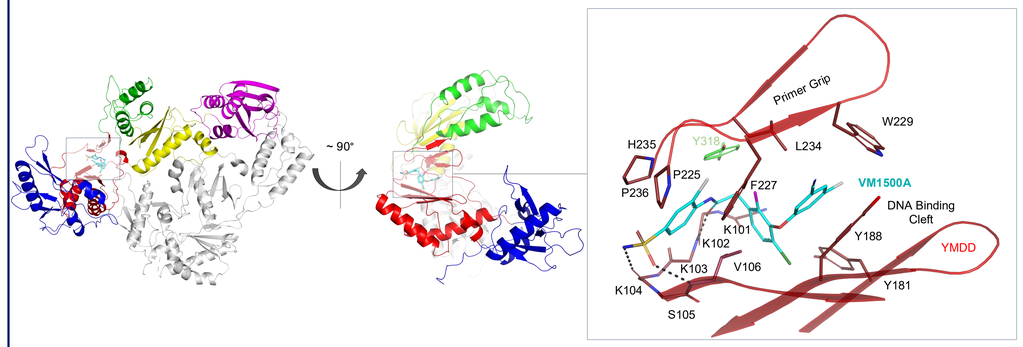
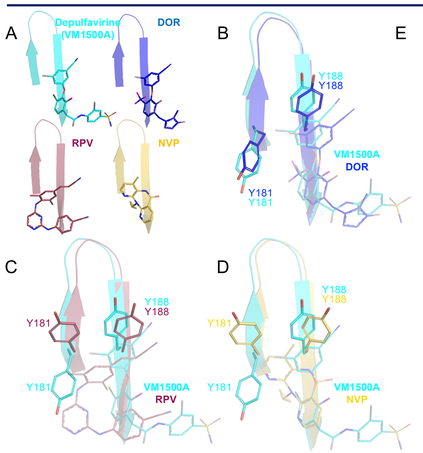


Fig 4: The X-ray crystal structure of the HIV-1 RT–VM1500A complex. The p51 subunit is depicted in white, and the p66 subunit is shown in multicolor: fingers (blue), palm (red), thumb (green), connection (yellow) subdomains, and the RNase H domain (purple). Depulfavirine (VM1500A) is shown in cyan and colored by atom, with Cl in gray, F in magenta, Br in green, S in yellow, O in red, and N in blue, and binds within the NNRTI-binding pocket of HIV-1 RT. Hydrogen bond interactions between Depulfavirine and RT residues are indicated by black dashed lines. This structure has been deposited in the Protein Data Bank under accession code 7TAZ.

Distinct Conformations of Y181 Across NNRTI–RT Complexes



VM1500A	DOR	RPV	NVP
	L100	L100	L100
K101	K101	K101	K101
K102			
K103	K103	K103	
K104			
S105			
V106	V106	V106	V106
V108	V108		
		V179	V179
		Y181	Y181
Y188	Y188	Y188	Y188
		G190	G190
P225	P225		
F227	F227	F227	F227
W229	W229	W229	W229
L234	L234	L234	L234
H235	H235	H235	H235
P236	P236	P236	P236
Y318	Y318	Y318	Y318

Figure 5. Distinct Conformations of Y181 Across NNRTI–RT Complexes. Structural comparisons showing how different NNRTIs position Y181 within the HIV-1 reverse transcriptase (RT) NNRTI-binding pocket. (A) Overlay of VM1500A (cyan, PDB 7TAZ), DOR (blue, PDB 4NCG), RPV (rust, PDB 3MEE), and NPV (yellow, PDB 1VRT) aligned on the NNRTI-binding pocket. (B) Comparison of depulfavirine (VM1500A) and DOR interactions with RT. (C) Structural comparison of depulfavirine (VM1500A) and RPV. (D) Structural comparison of depulfavirine (VM1500A) and NPV. (E) Summary of key NNRTI–RT interactions between the various NNRTIs.

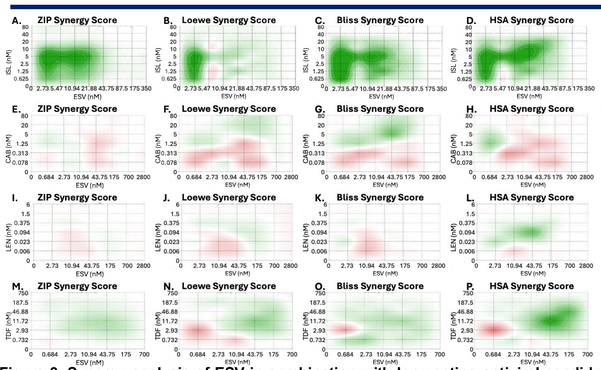
Key Findings

Depulfavirine inhibits HIV-1 reverse transcriptase through a distinct binding mode that supports activity against resistant variants and compatibility with combination and long-acting ART strategies.

Conclusions

- Depulfavirine binds HIV-1 reverse transcriptase in an extended NNRTI binding mode within the NNRTI pocket.
- This binding mode supports broad antiviral activity across multiple NNRTI-resistant RT variants.
- Reduced susceptibility is primarily associated with mutations involving F227, consistent with structural and biochemical data.
- Elsulfavirine, the prodrug of depulfavirine, demonstrates additivity when combined with long-acting antivirals and standard ART agents.
- These findings support depulfavirine's potential utility in both combination and long-acting antiretroviral therapy strategies.

Long-Acting Combination Strategies Involving Elsulfavirine (Prodrug of Depulfavirine)



Q.

	Average ZIP Synergy Score	Average Loewe Synergy Score	Average Bliss Synergy Score	Average HSA Synergy Score
ESV + ISL	**8.24** p=1.93e-08	**3.98** p=8.38e-04	**9.15** p=9.24e-09	**8.74** p=2.20e-12
ESV + CAB	**-0.54** p=8.47e-01	**-0.26** p=9.35e-01	**1.05** p=7.26e-01	**-1.15** p=7.27e-01
ESV + LEN	**-0.28** p=7.75e-01	**-0.40** p=6.20e-01	**-0.47** p=7.08e-01	**1.71** p=2.95e-02
ESV + TDF	**2.7** p=3.10e-03	**1.84** p=9.19e-02	**2.97** p=4.06e-03	**4.19** p=1.74e-04

Figure 3. Synergy analysis of ESV in combination with long-acting antiviral candidates. Synergy scores were calculated at each individual dose–response point and as overall synergy scores using the ZIP, Loewe, Bliss, and HSA models. Drug combinations tested included **ESV+ISL, ESV+CAB, ESV+LEN, and ESV+TDF**. Assays were performed in TZM-GFP cells, with dose–response matrices pre-incubated with cells for 24 h prior to infection. Cells were then infected with NL4-3 Δenv pseudotyped virus, and GFP expression was imaged 48 h post-infection. Percent inhibition values were calculated and analyzed using SynergyFinder Plus. Two-dimensional synergy plots are shown in panels A–P, with synergy scores summarized in table format in panel Q (18).

In Vitro Resistance to Depulfavirine (VM1500A)

A

	HIV-1 RT Resistance *in vitro* Fold-change compared to WT (SD)
	VM1500A
WT	1
Y181C	1.77 (0.7)
V106A	1.56 (1.0)
F227C	8.83 (4.7)
V106AF227C	12.39 (5.7)
K103N	1.28 (1.6)

B

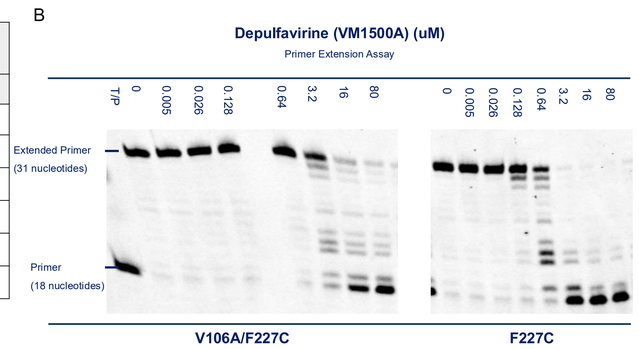


Figure 6. In vitro resistance profile of depulfavirine (VM1500A) against NNRTI-resistant HIV-1 reverse transcriptase. A) Fold-change in inhibitory potency of VM1500A relative to wild-type (WT) HIV-1 RT for selected NNRTI-resistance mutations, shown as mean ± SD. B) Representative primer extension assays illustrating depulfavirine inhibition of mutant RT enzymes, including F227C and the V106A/F227C double mutant, across increasing concentrations of depulfavirine. Fully extended and unextended primer products are indicated. Quantification from at least three independent experiments was used to determine IC_{50} values.

Acknowledgments

[1]Laboratory of Biochemical Pharmacology, Department of Pediatrics, Emory University School of Medicine, Atlanta, GA
[2]Children's Healthcare of Atlanta, Atlanta, GA
*Correspondence (stefanos.sarafianos@emory.edu)

This work was funded in part by the National Institutes of Health (F31AI172618, R01AI076119, R37AI076119, and U54AI170855; A.A.S. was supported in part by GM135060). The content is solely the responsibility of the authors and does not necessarily represent the official views of the National Institutes of Health. S.G.S. acknowledges funding from the Nahmias-Schinazi Distinguished Chair in Research. X-ray crystallography data were collected at the Advanced Photon Source, Argonne National Laboratory (Beamline 22-ID-D). Graphic Images were created with Pymol. The compounds elsulfavirine and depulfavirine (VM1500A) were provided by Viriom, Inc.

References

1. HIVinfo.NIH.gov. FDA-Approved HIV Medicines 2025 [Available from: https://hivinfo.nih.gov/understanding-hiv/fact-sheets/fda-approved-hiv-medicines.
2. Ravichandran SM, McFadden WM, Snyder AA, Sarafianos SG. State of the ART (antiretroviral therapy): Long-acting HIV-1 therapeutics. Global Health & Medicine. 2024;6(5):285-94.
3. Tailor MW, Chahine EB, Koren D, Sherman EM. Lenacapavir: a novel long-acting capsid inhibitor for HIV. Annals of Pharmacotherapy. 2024;58(2):185-95.
4. UNAIDS. Global HIV & AIDS statistics — Fact sheet 2024 [Available from: https://www.unaids.org/en/resources/fact-sheet.
5. Al-Salama ZT. Elsulfavirine: First global approval. Drugs. 2017;77(16):1811-6.
6. Viriom. Pipeline: Viriom; 2025 [Available from: https://www.viriom.com/pipeline.
7. Javanbakht H, Ptak R, Chow E, Yan J, Russell J, Mankowski M, et al. In vitro resistance development for RO-0335, a novel diphenylether nonnucleoside reverse transcriptase inhibitor. Antiviral research. 2010;86(2):212-9.
8. Sarafianos SG, Marchand B, Das K, Himmel DM, Parniak MA, Hughes SH, et al. Structure and function of HIV-1 reverse transcriptase: molecular mechanisms of polymerization and inhibition. Journal of molecular biology. 2009;385(3):693-713.
9. De Clercq E. The role of non-nucleoside reverse transcriptase inhibitors (NNRTIs) in the therapy of HIV-1 infection. Antiviral research. 1998;38(3):153-79.
10. Singh K, Marchand B, Kirby KA, Michailidis E, Sarafianos SG. Structural aspects of drug resistance and inhibition of HIV-1 reverse transcriptase. Viruses. 2010;2(2):606-38.
11. Le GRICE SF, GRÜNINGER-LEITCH F. Rapid purification of homodimer and heterodimer HIV-1 reverse transcriptase by metal chelate affinity chromatography. European journal of biochemistry. 1990;187(2):307-14.
12. Michailidis E, Marchand B, Kodama EN, Singh K, Matsuoka M, Kirby KA, et al. Mechanism of inhibition of HIV-1 reverse transcriptase by 4'-ethynyl-2-fluoro-2'-deoxyadenosine triphosphate, a translocation-defective reverse transcriptase inhibitor. Journal of Biological Chemistry. 2009;284(51):35681-91.
13. Kabsch W. xds. Acta Crystallographica Section D: Biological Crystallography. 2010;66(2):125-32.
14. McCoy AJ, Grosse-Kunstleve RW, Adams PD, Winn MD, Storoni LC, Read RJ. Phaser crystallographic software. Journal of applied crystallography. 2007;40(4):658-74.
15. Winn MD, Ballard CC, Cowtan KD, Dodson EJ, Emsley P, Evans PR, et al. Overview of the CCP4 suite and current developments. Acta Crystallographica Section D: Biological Crystallography. 2011;67(4):235-42.
16. Emsley P, Cowtan K. Coot: model-building tools for molecular graphics. Acta crystallographica section D: biological crystallography. 2004;60(12):2126-32.
17. Liebschner D, Afonine PV, Baker ML, Bunkóczi G, Chen VB, Croll TI, et al. Macromolecular structure determination using X-rays, neutrons and electrons: recent developments in Phenix. Acta Crystallographica Section D: Structural Biology. 2019;75(10):861-77.
18. Zheng S, Wang W, Aldahdooh J, Malyutina A, Shadbahr T, Tanoli Z, et al. SynergyFinder plus: toward better interpretation and annotation of drug combination screening datasets. Genomics, Proteomics and Bioinformatics. 2022;20(3):587-96.